Effect of pulp density on acidulation mechanisms in low-grade phosphate rock using biogenic acid generated by *Acidithiobacillus thiooxidans*.

Sandra Milena Restrepo Arcila[1,2], Henry Alonso Colorado Lopera[2], Marco Antonio Márquez Godoy[1]

[1] Facultad de Minas, Departamento de Materiales y Nanotecnología, Universidad Nacional de Colombia–Medellín
[2] CCComposites Laboratory, Universidad de Antioquia UdeA, Calle 70 N°. 52-21, Medellín, Colombia.
*Email: srestrepoar@unal.edu.co (S. M. R. Arcila)

Abstract

Phosphorus is essential for global food security, but traditional extraction using thermal and hydrometallurgical methods is hampered by the depletion of deposits and high energy costs. This study evaluates the recovery of low-grade Colombian phosphate rock (5.5% w/w P) through biogenic leaching. Unlike chemical acidulation, which consumes a lot of water and tends to produce disruptive foam, this biotechnological approach offers a controlled and sustainable alternative.

A biological leaching agent was obtained using *Acidithiobacillus thiooxidans* (ATCC 13977), with systematic control of pH, sulfate generation, and biomass kinetics. The process was tested with pulp densities of 20% and 30% (w/w). Comprehensive characterization using XRF, XRD, FTIR, and SEM-EDS revealed significant mineralogical transformations and morphological changes in the residues. UV-Vis spectroscopy confirmed the effective solubilization of P.

By operating at room temperature and replacing concentrated chemical reagents, this method significantly reduces the carbon and water footprint. The results demonstrate that bioleaching is a technically viable circular approach to transforming mineral waste into strategic nutrients. This research promotes technological sovereignty and industrial sustainability by providing an efficient way to use low-value natural resources.

Keywords

Bioleaching, *Acidithiobacillus thiooxidans*, Low-grade Phosphate Rock, Solubilization Efficiency, Circular economy.

Graphical abstract

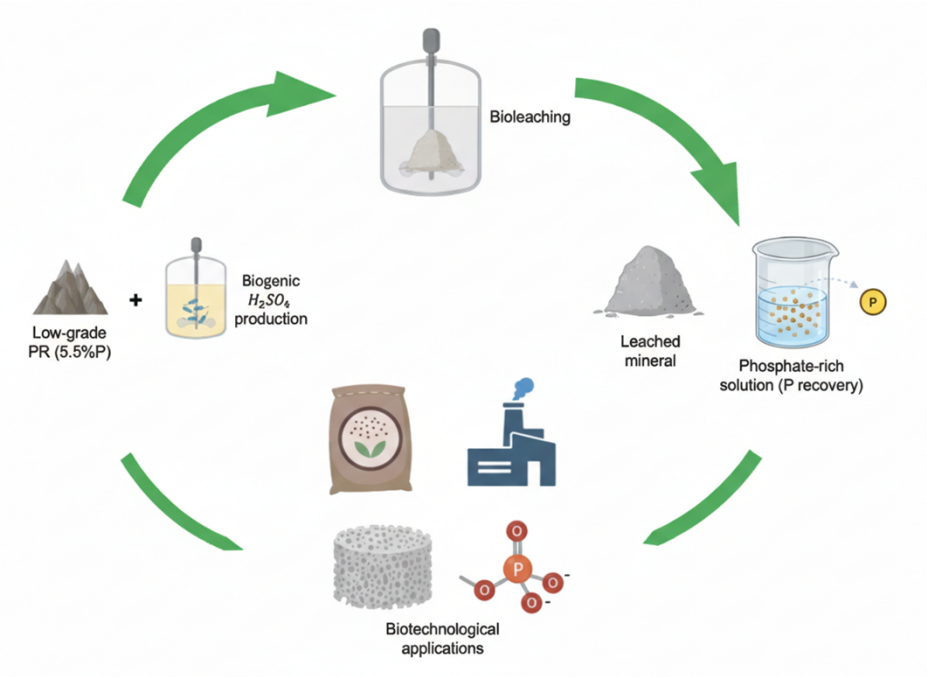

1. Introduction

Phosphoric acid is an essential raw material in various industries, such as agriculture for the manufacture of fertilizers, medicine, the military, food, metallurgy, and geopolymers [1], [2], and everyday life [3], [4], [5], [6]. The main raw material in conventional phosphoric acid production is phosphate rock (PR), around 80% of which is extracted from deposits [7]. Global phosphate reserves amount to approximately 70 billion tons, of which Morocco has the largest share, with reserves of 50 billion tons, representing 71.43% of the world total [8]. The main phosphate-producing countries are China, Morocco, the United States, and Russia, which together account for 79% of global production [9]. Other countries such as Brazil, Jordan, Egypt, and Saudi Arabia contribute to the rest of phosphate production, supplementing the global supply of this vital resource. Figure 1 shows global production by country during 2024 [10].

Phosphate rock resources are classified into five main types of deposits, among which marine sedimentary deposits stand out, representing approximately 75% of global sources. These are followed by igneous, metamorphic, and weathered deposits (15-20%) and, finally, biogenic sources (2-3%) [8] [11]. Commercial-grade minerals obtained from sedimentary and igneous sources have P_2O_5, content of 28-36% and 35-39%, respectively. Depending on the P_2O_5, concentration, the mineral is classified into three grades: high (26-35%), medium (17-25%), and low (12-16 %) [12].

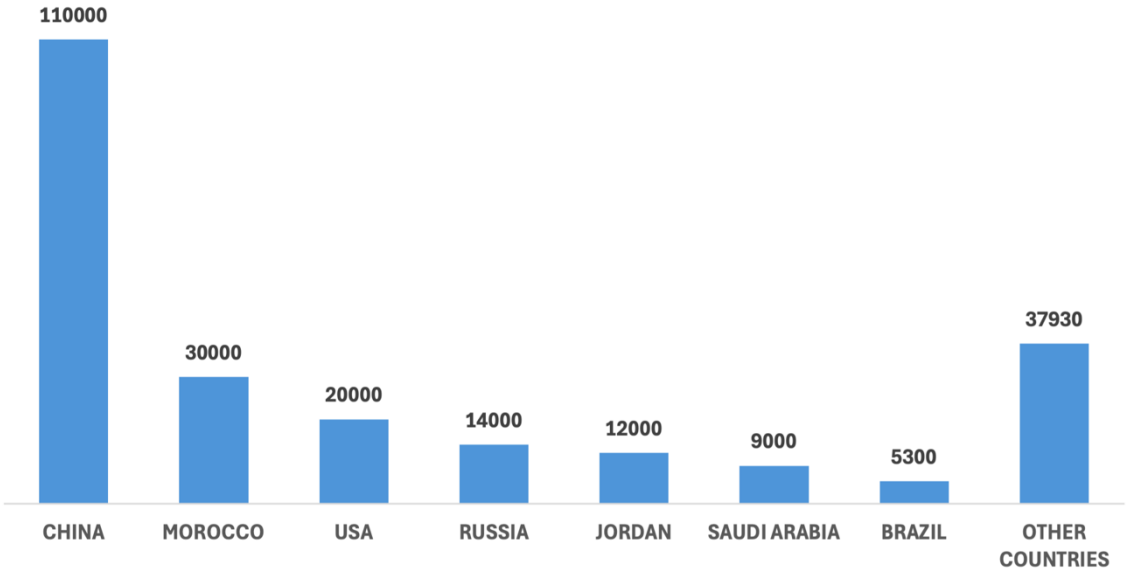

Figure 1. Worldwide production of phosphate rock for the year 2024 (in thousands of metric tons).

Igneous deposits, being a secondary source, are characterized by low-grade phosphate minerals, with a P_2O_5 content ranging from 5% to 15%. Similarly, the concentrate obtained through the processing and beneficiation of igneous phosphate has a lower content of carbonates and contaminants compared to certain sedimentary phosphate rocks [13]. Therefore, to treat PR ore in phosphoric acid production, processing methods are used that include thermal and hydrometallurgical methods [14]. The thermal method is an important technique in phosphate production, accounting for more than 10% of marketable phosphates worldwide [15], It consists of calcining the ore at a temperature close to 950 °C, at which point the calcareous minerals are transformed into CaO and MgO releasing CO_2. The ore is then cooled, generally using NH_4Cl o NH_4NO_3 at a concentration of around 5% to form $Ca(OH)_2$ and $Mg(OH)_2$ which are then discarded using a hydrocyclone process, thus achieving a high-quality phosphate concentrate [16]. This method is also widely used for the beneficiation of rare earth elements present in phosphate minerals, such as monazite [17]. Despite the effectiveness of this method for phosphate rock processing, calcination has a critical limitation, as the thermal requirements of this process can double the total energy consumed in the physical beneficiation of phosphate minerals. This requirement limits its economic viability to regions with access to low-cost energy sources and limited water resources, as is the case with several deposits in the Middle East [18]. Hydrometallurgical methods include acid leaching and bioleaching. In the former, the reaction with sulfuric acid produces approximately 95% phosphoric acid [3]. During this process, in addition to phosphoric acid, gypsum ($CaSO_4$) is obtained as a by-product [19], according to reaction 1.

$$Ca_5F(PO_4)_3 + 5H_2SO_4 + 5nH_2O \rightarrow 3H_3PO_4 + 5CaSO_4.nH_2O + HF \quad (1)$$

One of the main challenges of these wet reactions is the significant amount of foam generated by the acid hydrolysis reaction with dolomite $CaMg(CO_3)_2$, and calcite $CaCO_3$, present in the PR (reactions 2, 3 y 4), which hinders production efficiency and increases process costs. To optimize this process and control foaming, studies have been presented on the use of defoamers as agents that significantly reduce its formation [20].

$$CaCO_3 + H_2SO_4 \rightarrow CaSO_4 + H_2O + CO_2\uparrow \quad (2)$$

$$CaCO_3.MgCO_3 + H_2SO_4 \rightarrow CaSO_4 + MgSO_4 + 2H_2O + 2CO_2 \quad (3)$$

$$MgCO_3 + 2H_3PO_4 \rightarrow Mg(H_2PO_4)_2 + CO_2 + H_2O \quad (4)$$

On the other hand, the use of biotechnology and bioleaching is gaining momentum, providing unconventional and sustainable treatments that help reduce waste emissions and, in this case, using microorganisms in the solubilization of phosphorus [21]. Acidophilic bacteria, particularly species such as *Acidithiobacillus thiooxidans* and *Leptospirillum ferriphilum*, thrive in extreme environments such as sulfurous mines and sulfur-rich lagoons [22], where their chemoautotrophic metabolism allows them to oxidize inorganic compounds (sulfides and iron) and produce organic acids biogenically [23], [24]. In the laboratory and on a small scale, these bacteria are used in various biotechnological processes: in bioleaching for the recovery of metals such as copper, nickel, and rare earth elements, among others, from low-grade ores [25]; in the bioremediation of acid mine drainage, using microbial consortia such as acidophilic sulfate-reducing bacteria (*Desulfosporosinus spp, Acidithiobacillus spp.*) which suppress acidity and allow heavy metals to precipitate [23], [26]; and in effluent treatment, where bioreactors with lignocellulosic substrates achieve sulfate reduction efficiencies of over 68% and remove heavy metals such as Fe, Cd, Zn, and Cu with efficiencies between 94% and 99% [27], [28], [29]. In addition, the microbial symbiosis between chemolithotrophic acidophiles and sulfate-reducing bacteria optimizes the efficiency of the process by raising the pH and promoting the coprecipitation of metals through the generation of sulfide [30]. Thanks to their ability to synthesize organic acids endogenously and function without additional chemical inputs, these bacteria are sustainable biocatalysts with great potential in biohydrometallurgy, acid water bioremediation, and selective metal recovery on a laboratory scale. In Colombia, previous studies [31], [32] show how a strain of *Acidithiobacillus thiooxidans* capable of solubilizing elemental sulfur according to equation 5 to produce sulfuric acid, which when reacting with an RF in concentrations of 10%, 15%, 20%, and 25%, effectively solubilizes 100% of the phosphorus in a two-step method in a 500 ml Erlenmeyer flask "growth and then recovery" in a time of 29 days.

$$S^0 + \frac{3}{2}O_2 + H_2O \rightarrow H_2SO_4 \quad (5)$$

This study focused on the leaching of low-grade PR using sulfuric acid in a 5-liter reactor. The main objective was to maximize phosphorus solubilization while controlling foaming, a critical phenomenon resulting from the reaction of carbonates within the PR, by regulating the mixing conditions in a single step. A key parameter evaluated was pulp density, technically defined as the percentage ratio between the mass of solids (RF) and the total mass of the suspension (solid phase + liquid phase). In this research, pulp densities of 20% and 30% (w/w) were analyzed, which allowed the most favorable conditions to be determined for optimizing dissolution times and process efficiency. The characterization of the reaction products confirmed the effectiveness of the acid treatment in transforming the mineral phases present. The results show that, through rigorous process design and selection of optimal operating parameters, it is possible to efficiently recover low-grade phosphate resources, thereby contributing to their sustainable use in biotechnological applications.

2. Materials and methods

This work was carried out in the following stages:
A commercial sample of phosphate rock was purchased from the company Inferhuila. This rock has low assimilation (low concentration of (P_2O_5)) and comes in 50 kg packages from the Tesalia and Aipe deposits in the department of Huila. This was characterized mineralogically by particle size distribution (PSD), X-ray diffraction (XRD), X-ray fluorescence (XRF), and Fourier transform infrared spectroscopy (FTIR). All FTIR analyses were performed on a Shimadzu-8400S spectrophotometer, in a range of 400-4000 cm^{-1} and a resolution set for solid sample analysis at 4 cm^{-1}; the spectra were processed using IR Solution v.1.3 software. XRD (powder method) was performed for all samples using Rigaku Miniflex II equipment, with Cu $k\alpha 1$ sources and a nickel filter, 30 kV, 15 mA, and a graphite monochromator, a scanning angle of 2θ between 3° and 70°, using the step-by-step method, with a step of 0.02° and 0.5 s per step. The diffractograms were processed using X'pert HighScore Plus version 3.0 software, with semi-quantification using the Rietveld method. The XRF analyses were performed using a Thermo Fisher Scientific spectroscope, using the X UQ Helium method, calculating the elements present in the samples in the form of oxides. The morphology and micro-elemental composition of the PR and leached samples were analyzed using scanning electron microscopy with energy dispersive X-ray spectroscopy (SEM-EDS) on a JEOL JSM-6490 microscope under high vacuum conditions and with samples sputter-coated with a thin film of gold.

The biogenic acid was produced using a strain of the microorganism A. thiooxidans from the American Type Culture Collection (ATCC 13977), which was grown in 9K medium [33] with the following composition: 16.667 g/L of $(NH_4)_2SO_4$, 2.778 g/L K_2HPO_4, 2.778 g/L $MgSO_4.7H_2O$, 0.556 g/L KCl and 0.056 g/L $Ca(NO_3)_2.5H_2O$, in a stirred tank bioreactor with an effective volume of 5 L, using 4.5 L of distilled water, 10% of the inoculum volume, and 4% S_0. The pH was adjusted to 1.8, temperature to 30°C, bioreactor aeration to 0.3 vvm (corresponding to 1.5 L/min), and agitation speed to 300 rpm for 21 days. During the process, pH, dissolved oxygen (DO), biomass, and amount of sulfates obtained were monitored every 3 days.

In order to solubilize the phosphorus present in the rock, a ratio of 20% and 30% P/V ratio of pulp, to which biogenic sulfuric acid was added, in a 5-liter bioreactor, at a stirring speed of 300 rpm, without aeration, taking aliquots approximately every 2.5 min. The amount of sulfates and phosphorus was determined for each aliquot using a Thermo Scientific Genesis 10 UV spectrometer, using ASTM D516-16 [34], at a wavelength of 420 nm for sulfate and the method described in Standard Methods for the Examination of Water and Wastewater 4500-P C, at a wavelength of 470 nm, for the determination of phosphates.

3. Results

a) Characterization de la RF

Initially, a granulometric analysis was performed on the PR sample according to ASTM C429-01 [35] with a total weight of 500 grams, processed by mechanical sieving with mesh sizes between 2.0 mm (10 mesh) and <0.08 mm (400 mesh bottom), in order to characterize the particle size distribution, a fundamental parameter for transformation processes, chemical reactivity, and unit operation design. Table 1 presents the results of the size distribution in terms of weight retained per granulometric fraction.

Table 1. Size distribution

Mesh	Opening (mm)	Weight retained (g)	Wt% Retained	% Accumulated passes
10	2	0	0.00%	100.00%
16	1.18	0	0.00%	100.00%
35	0.5	66	13.20%	86.80%
50	0.3	82	16.40%	70.40%
100	0.15	87	17.40%	53.00%
200	0.08	141	28.20%	24.80%
Bottom	<0.08	124	24.80%	0.00%
Total	—	500	100.00%	—

The analysis indicates that more than 50% of the material is composed of particles smaller than 0.15 mm, reflecting a predominantly fine distribution, which is desirable for the acidulation process where a high surface area is required.
Figures 2, 3, and Table 2 present the results for FTIR, XRD, and XRF, respectively. In the FTIR spectrum (Figure 2), the functional groups corresponding to silicates, phosphates, and carbonates present in the phosphate rock were identified. The representative bands are attributed to the frequencies of the carbonate ion $(CO_3)^{2-}$ with four vibrational modes corresponding to ν_3 at wavelengths of 1409 and 1460 cm^{-1}, followed by ν_2 at 874 cm^{-1}, ν_4 at 725 cm^{-1}, and $\nu_{1+}\nu_4$ at 1805 cm^{-1} [36], [37]. The bands of the phosphate ion $(PO_4)^{-3}$, in the vibrational modes ν_1 (very weak) in the spectral region of 963 cm^{-1}, ν_2 at 471 cm^{-1}, ν_3 from 1000 to 1150 cm^{-1}, and ν_4 between 540 and 620 cm^{-1} [38], [39].

The PR was classified granulometrically into three fractions: retained on a 100-mesh screen, between 100 and 200 mesh screens, and passing through a 200-mesh screen. Each fraction was subsequently analyzed by XRD to identify and semi-quantify the mineral phases present. Semi-quantitative analysis of the overall sample indicated that the main mineral phases were calcite (40.4%), dolomite (39.0%), and carbonate-fluorapatite (20.4%), with a minor presence of quartz (0.2%). The spectra shown in Figure 3 reveals that the fraction retained on the 100 mesh (Figure b) shows a higher relative content of calcite, as well as a slight increase in the proportion of fluorapatite, similar to that observed in the finest fraction (passing through the 200 mesh, Figure d). In contrast, the intermediate fraction (between 100 and 200 mesh) exhibits the lowest proportion of calcite, suggesting possible mineralogical segregation based on particle size.

Elemental analysis of the PR sample revealed a high concentration of calcium (48.14%), followed by magnesium (6.38%), phosphorus (5.59%), silicon (3.05%), and other elements present in smaller proportions (<1%). This composition suggests that it is a commercial phosphate rock with a high carbonate content and a low proportion of phosphates.

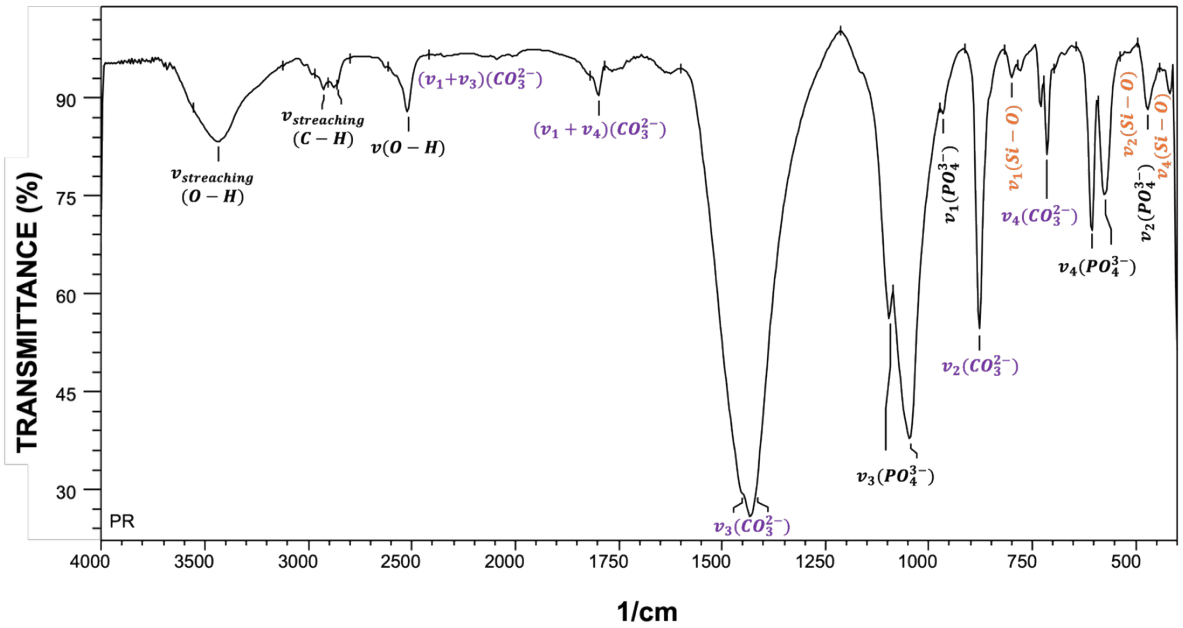

Figure 2. FTIR spectrum of commercial PF, (ν_1 corresponds to the band related to symmetric stretching, ν_2 to stretching, ν_3 to antisymmetric stretching, and ν_4 bending).

Table 2. Results of X-ray fluorescence spectroscopy (XRF) of commercial PR (LOI 28.53).

Mineral	Element	Ca	Mg	P	Si	Fe	Al	Sr	K	S	Mn	Ti	Cu
PR	Wt%	48.14	6.38	5.59	3.05	0.443	0.575	0.205	0.102	0.07	0.04	0.029	0.052

b) Biogenic sulfuric acid

Figure 4 presents the analysis of the variables evaluated throughout the experimental process, showing the significant biochemical interactions between microbial activity and the physicochemical parameters of the system. Figure 4a) shows an inverse correlation between sulfate concentration and pH, consistent with the generation of sulfuric acid as a byproduct of microbial metabolism, which explains the progressive acidification of the medium. Likewise, electrical conductivity increased over time, showing a direct correlation with sulfate accumulation, attributable to the increase in the concentration of ionic species in solution [32], [40]. At the same time, in 4b), a directly proportional correlation was observed between the concentration of sulfates and the number of cells, indicating that sulfate production is associated with the biological process of microbial oxidation of reduced sulfur compounds by *Acithiobacillus thiooxidans*. Finally, the decrease in dissolved oxygen coincided with the exponential growth of biomass, reflecting intense aerobic metabolic activity. The maximum sulfate concentration reached in this process was 100074 mg/L, corresponding to an approximate yield of 85% of the theoretical value expected for the single-step reaction in a matter of minutes.

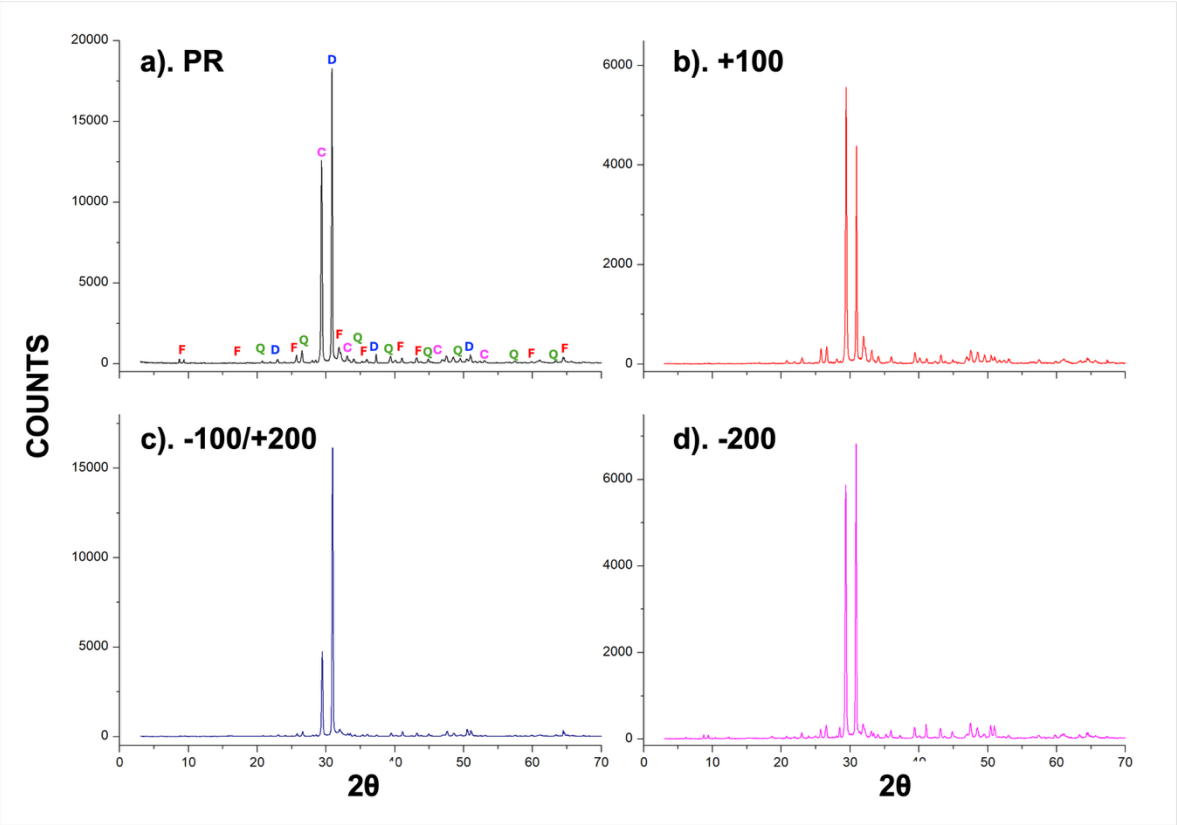

Figure 3. XRD spectrum of phosphate rock showing the minerals identified: C-calcite ICSD 96-900-1298, D-dolomite ICSD 96-900-1246, F-carbonate-fluorapatite ICSD 98-007-1854, Q-quartz ICSD 98-008-9290.

c) Phosphorus solubilization process

Figure 5 shows the behavior of phosphate mineral solubilization under two different concentrations by monitoring the concentration of sulfates, soluble phosphorus, and pH over time.

Under both experimental conditions, a sharp decrease in sulfate concentration (black line) was recorded during the initial stage of the process (0–5 min). Rather than a surface dissolution effect, this phenomenon suggests the immediate precipitation of gypsum ($CaSO_4.2H_2O$) upon contact between the biogenic sulfuric acid and the calcium-rich phosphate rock. The high availability of Ca^{2+} ions released from the mineral matrix likely exceeded the solubility product of calcium sulfate, leading to rapid mineral scale formation. Following this initial depletion, sulfate levels remained relatively stable, indicating a state of chemical equilibrium in the liquid phase. Conversely, phosphorus release (magenta line) exhibited a steady progressive increase, reaching a maximum concentration near 5.400 mg/L. This corresponds to a solubilization efficiency exceeding 98.7% in both cases, demonstrating that despite the initial sulfate consumption for gypsum formation, the biogenic acid remained highly effective for phosphate matrix breakdown.

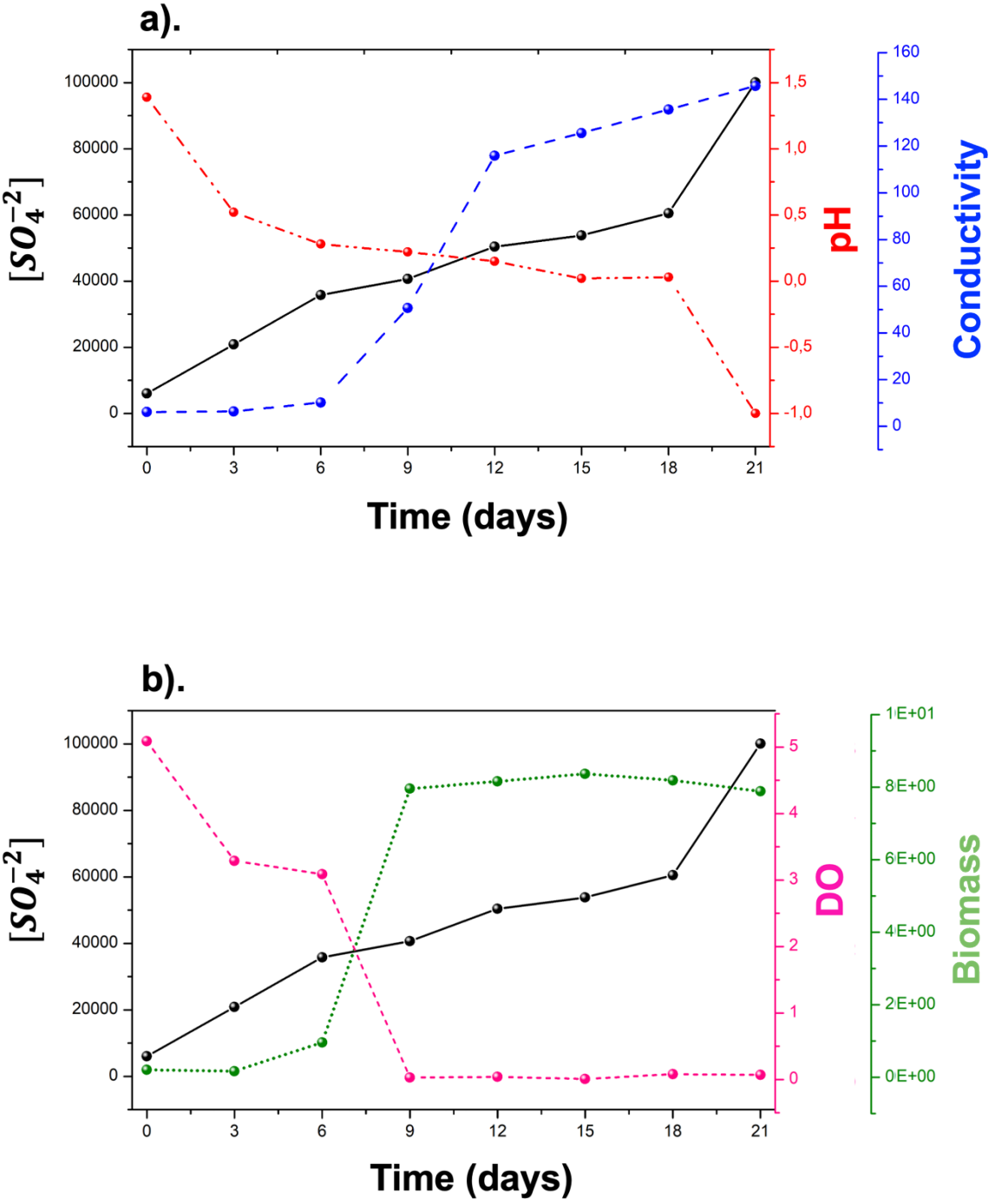

Figure 4. Comparison of parameter behavior in biogenic acid production over 21 days. a). Sulfates mg/L (black) vs. Conductivity μS/cm ((blue) and pH (red), b). Sulfates mg/L vs. dissolved oxygen (DO) mg/L (pink) and biomass cells/cm (green).

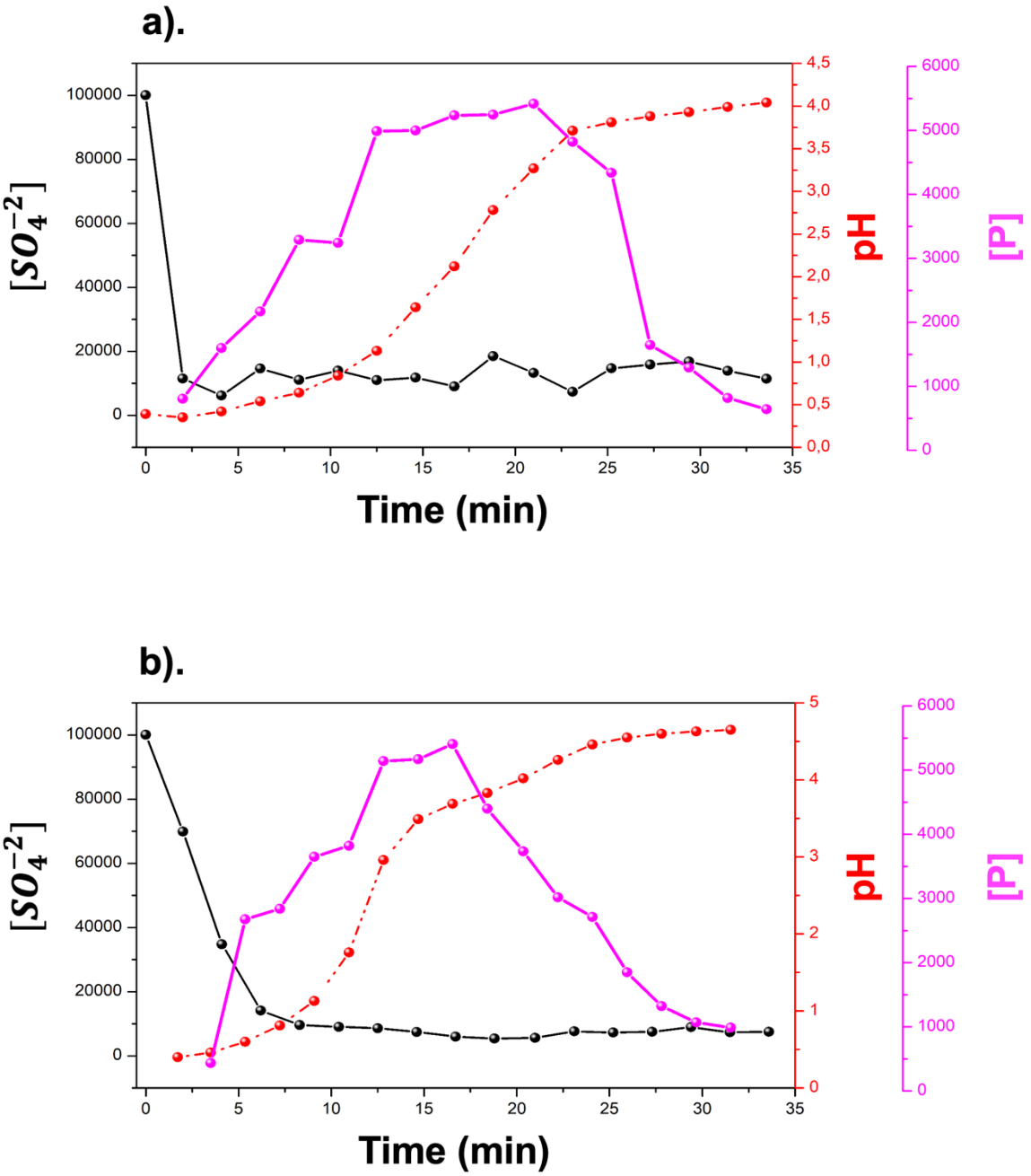

Figure 5. Pulp density PR, a). 20%. b). 30%. Solubilized phosphorus mg/L (magenta).

However, in the condition with 30% mineral concentration (5b), this maximum was reached in a significantly shorter time (17.6 min), while in the 20% condition (5a) the peak occurred at 22 minutes. From the above, it can be inferred that the system with the highest mineral concentration allowed for faster and more efficient phosphorus solubilization, probably due to greater availability of reactive sites or greater solid-liquid contact. On the other hand, the pH (red line) showed an upward trend in both conditions, inversely correlated with the release of phosphates, which alter the relative concentrations of the four polymorphs of

phosphoric acid [39], which could be associated with the neutralization of released acidic species or a dilution effect as equilibrium was reached.

Regarding the solid phase, its characterization and mineralogical composition by XRD, FTIR, FRX, and optics are presented in Figures 6, 7, 8, and 9, respectively. From Figure 6, it can be said that in both cases, characteristic patterns of well-defined crystalline phases are observed, with intense and sharp peaks centered mainly in the 2θ range between 25° and 35° (as in the initial sample). Comparative analysis suggests that, although both samples retain the main crystalline phase, the 20% leached sample underwent greater structural alteration, evidenced by the reduction in peak intensity and a possible increase in amorphous material. In contrast, the 30% sample retained greater crystallinity, which may be due to more superficial or less efficient leaching. This behavior is consistent with the previously analyzed kinetic data, where the 30% sample showed a faster phosphorus release peak, but did not necessarily imply greater overall mineral dissolution. Rietveld semi-quantitative analysis of the spectrum with 20% mineral shows that the sample is composed of dolomite 37.3%, calcite 33.5%, carbonate-fluorapatite 11.4%, coesite 13.8%, gypsum 3.8%, and wurtzite 0.2%. For the 30% sample, the composition is dolomite 34.7%, calcite 30.5%, carbonate-fluorapatite 14.4%, coesite 13.3%, gypsum 6.9%, and wurtzite 0.2%.

Figure 7 shows the FTIR spectra of the initial mineral and the leaching product for both concentrations. It is evident that the carbonate-fluorapatite has reacted to give way to the formation of gypsum (G) [31] as shown by the appearance of bands in the region of 600 and 660 cm^{-1} due to the bending vibration of the SO_4^2 group. On the other hand, an asymmetric stretching vibration was observed in the region of 1118 cm^{-1} due to the presence of the SO_4^2 group. The bands at 1622 cm^{-1} and 1687 cm^{-1} originated from the bending vibration of the $H-O-H$ group. The symmetric and asymmetric stretching vibration modes gave rise to peaks in the regions of 3398 and 3541 cm^{-1}. These stretching vibration bands originated from the presence of water [41]. Likewise, there is evidence of a decrease in certain bands belonging to the carbonates present in minerals such as calcite and dolomite. It can be noted that at the end of the reactions, the minerals mentioned above, which are resistant to the action of acid, are present without any apparent change, in addition to the reduction of the main mineralogical phases described and the appearance of a new phase such as gypsum.

Figure 8 shows the changes in the elemental composition of the PR after solubilization treatments at 20% and 30% pulp density. A significant decrease in calcium and phosphorus content was observed in both treated samples, confirming the effective dissolution of the mineral phases.

Figure 9 shows the microstructural transition of fluorapatite grains by SEM. Figure 9a) shows bacillary phosphate grains with elongated concretions or rounded bacillary habit and continuous surface, characteristic of a dense and crystalline mineral phase with significant primary porosity. The morphology shown in 9b) at a pulp density of 20% shows the onset of incipient zoning with the formation of microchannels, suggesting the diffusion of acid towards the core, selectively solubilizing the areas of greatest reactivity. Image 9c) also shows a degradation of the structure, where the volume of mineral removed has left a porous framework.

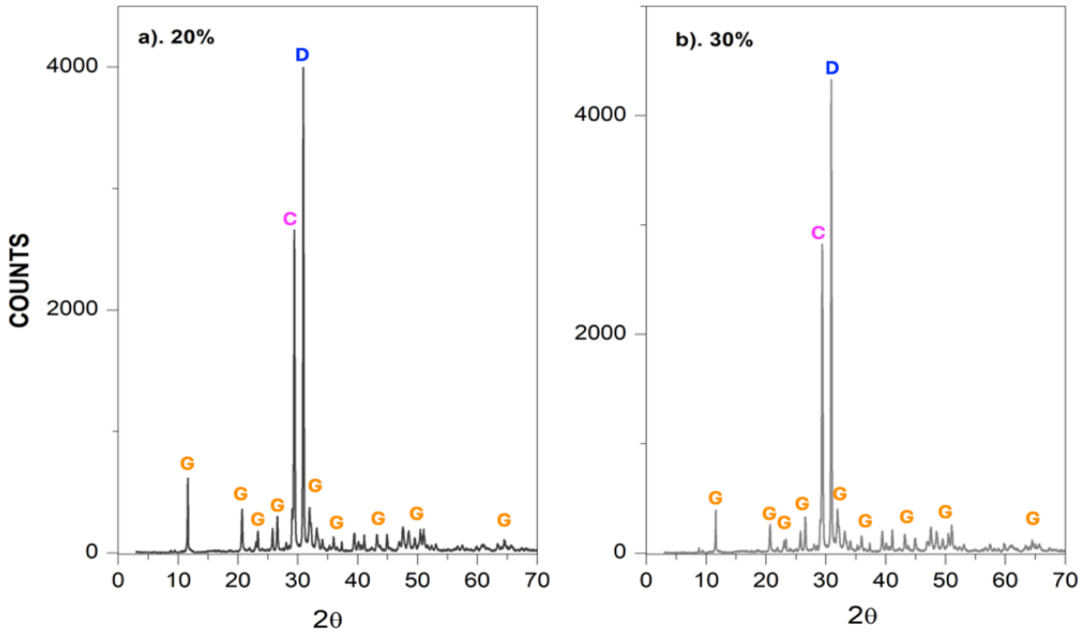

Figure 6. Comparison of XRD spectra for leached ore at pulp concentrations of a. 20%, b. 30%.

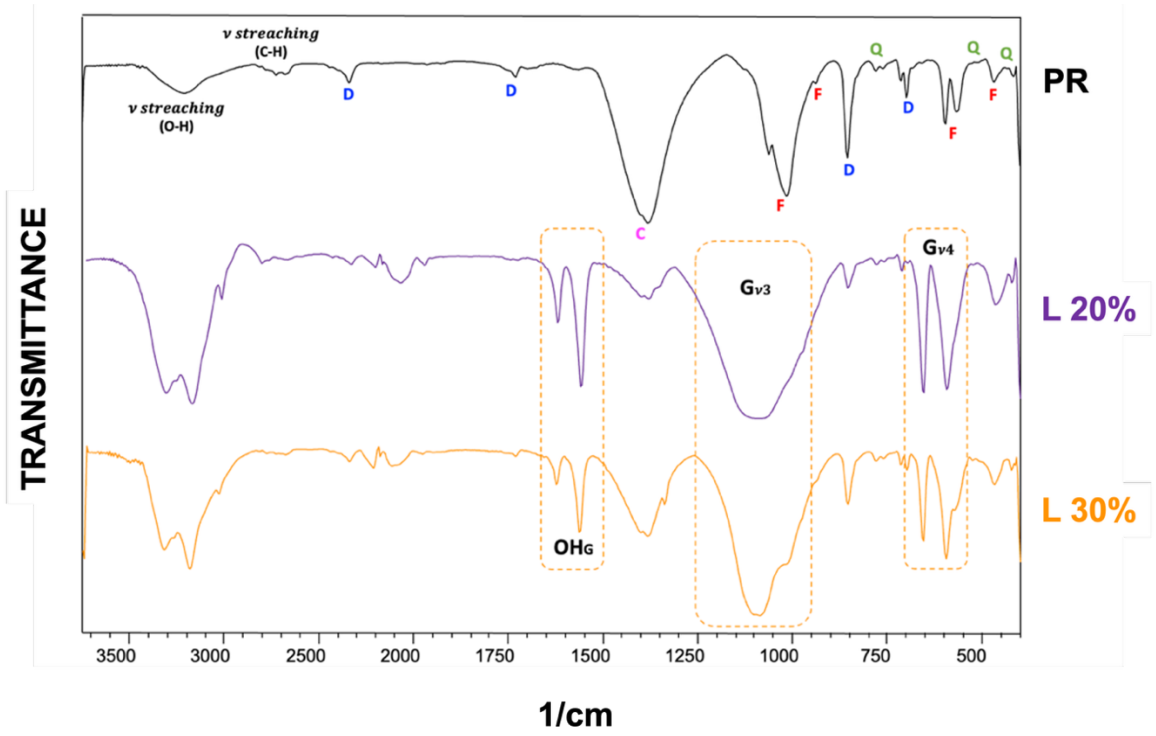

Figure 7. Comparative FTIR spectra of RF with both percentages of leached ore.

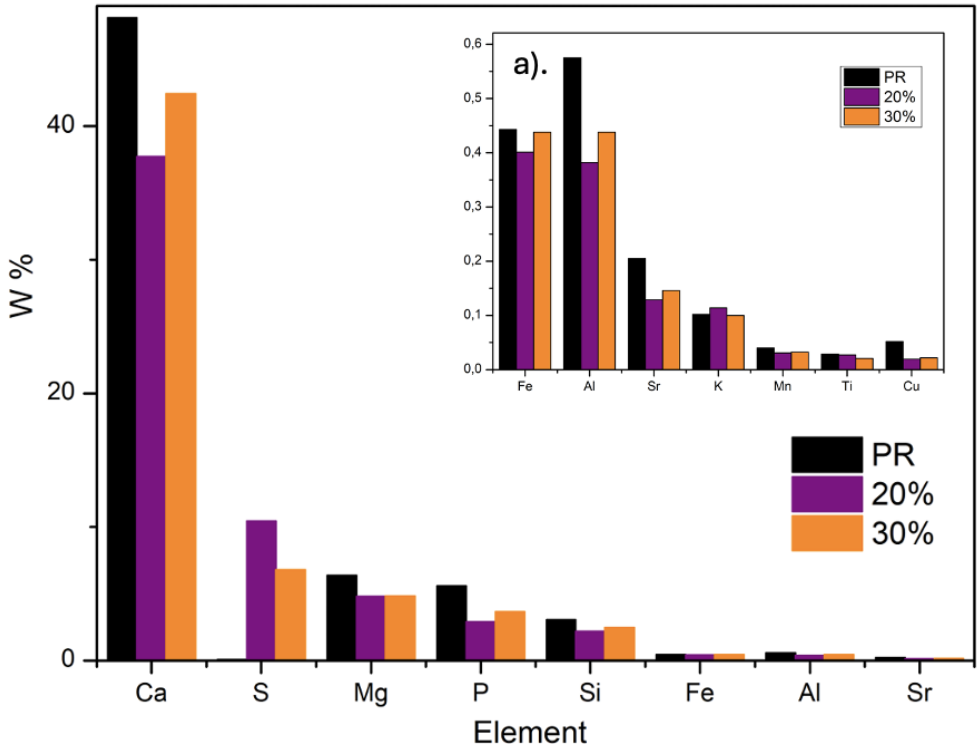

Figure 8. Comparative FRX results for initial RF and leaching residues at pulp densities of 20 and 30%. a) Trace elements.

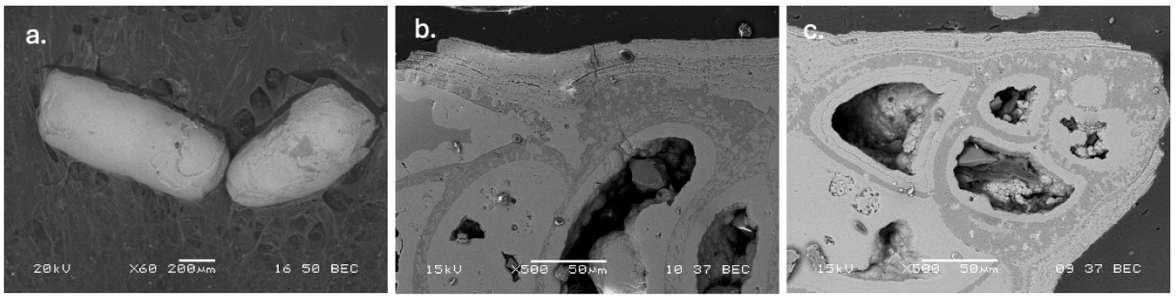

Figure 9. SEM of fluorapatite grains for the following conditions: a). initial PR sample, leaching product for a pulp density of b). 20% and c). 30%.

Figure 10 shows SEM-EDS images of the leached samples, detailing the heterogeneity of the chemical attack. Figure 10a). Spectra 1 and 2 with respect to the initial sample suggest deep decalcification and a drastic decrease in the percentage of P. Figure 10b). shows a highly differentiated core-shell structure. There is the formation of a passivation layer or accumulation of reaction products on the surface (brighter), composed of the precipitation of intermediate phases that trap P and Ca after the time of greatest solubilization of P according to Figure 5b. Meanwhile, in the inner matrix, deep solubilization of P can be observed, which shows in situ replacement of the original mineral by calcium sulfates, confirmed by the FRX result.

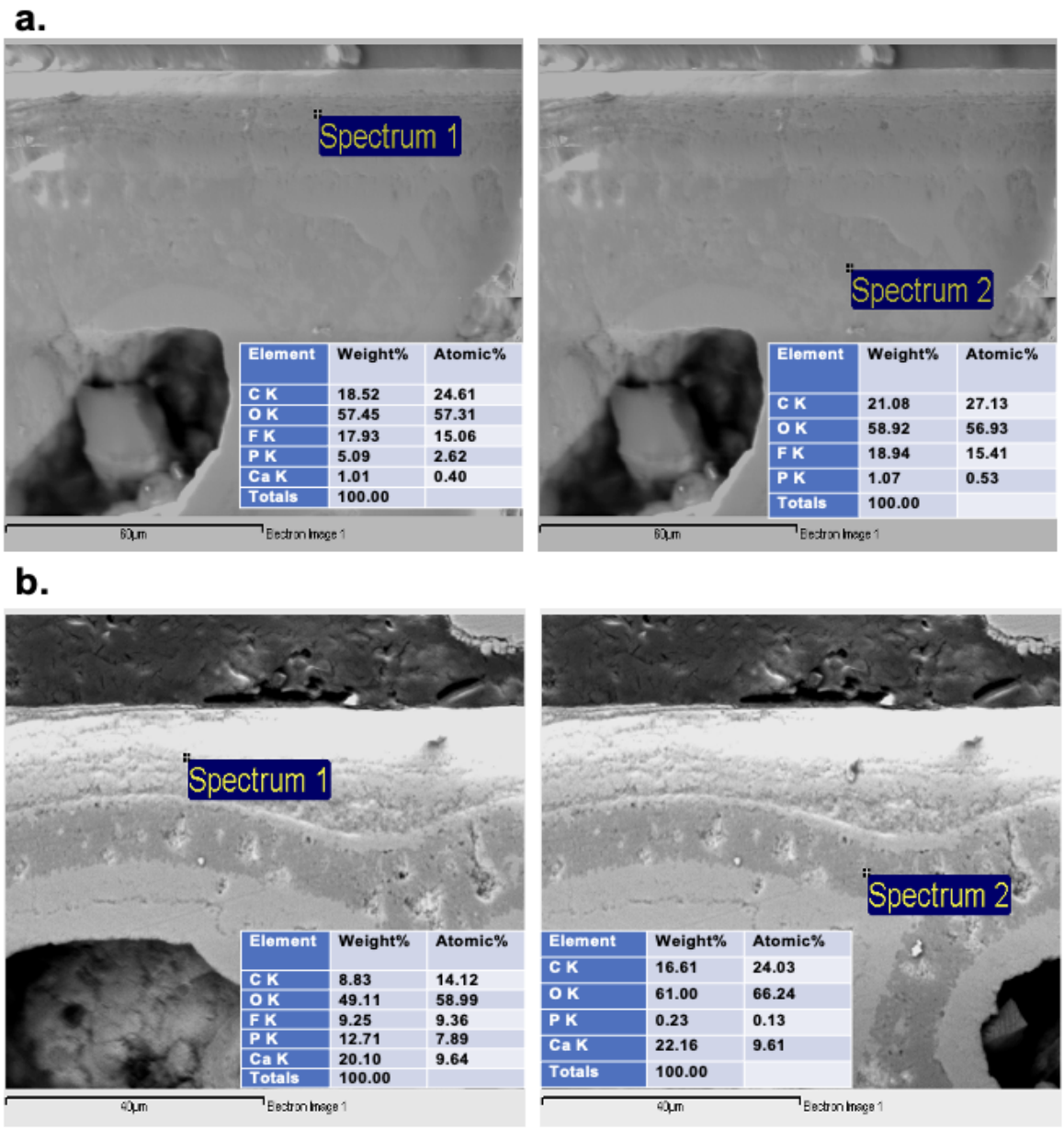

Figure 10. SEM-EDS leaching product for pulp density a). 20% and b). 30%.

4. Discussion

The transition to biotechnological processes in the phosphate industry not only responds to a need for energy efficiency but also aligns with the pillars of the circular economy and industrial decarbonization [42]. While the conventional thermal route is a high-impact linear model that relies on intensive combustion to reach calcination temperatures, biogenic leaching proposes a biorefinery model.

In this scheme, the use of *A. thiooxidans* acts as a biological catalyst that operates under mesophilic conditions, eliminating the direct carbon footprint associated with calcination furnaces. In addition, this route allows low-grade minerals that are currently discarded as

mining waste to be recovered and reintegrated into the fertilizer value chain. Therefore, microorganism-mediated solubilization constitutes a disruptive paradigm that transforms mineral waste into a strategic resource, minimizing the entropy of the process and maximizing the sustainability of the phosphate resource [43].

The interaction between the biogenic acid produced by *A. thiooxidans* and low-grade phosphate rock reveals complex leaching dynamics that transcend simple chemical solubilization. The transition from an original massive grain to skeletal structures in leached residues with a pulp density of 20% and 30% provides physical evidence of a process of mineral substitution by limited diffusion.

The behavior observed in the XRD for leached minerals under the two mineral pulp density conditions (Figure 6) can be explained in several ways. The most likely reason why the calcite did not react completely is that the sulfuric acid was completely depleted. A more remote possibility could have been the precipitation of gypsum, generating coating films that would have inhibited subsequent dissolution, as reported by other authors in natural systems [44], [45]. Dolomite, on the other hand, despite effervescing in acid, only does so abundantly at higher temperatures [46], [47], [48]. It is possible that the carbonate-fluorapatite did not dissolve completely, mainly due to the depletion of the leaching agent, although the formation of gypsum films that inhibit, at least partially, its dissolution cannot be ruled out. Another possible explanation for the minerals that did not react completely may have been that the large amount of gypsum formed [29] prevented complete homogenization between the acid and the rest of the mineral during stirring, as well as the reprecipitation of phosphorus during the reaction.

When comparing the FRX results (Figure 8) for pulp densities, the 20% (w/w) sample showed greater phosphorus removal, reaching a residual value of 2.92% compared to the initial 5.59%. This greater thoroughness in extraction suggests that a lower solid load optimizes the chemical potential of the biogenic leachate by reducing the early saturation of solutes in the liquid phase. Similarly, the notable increase in sulfur in the treated samples, especially in the 20% sample (10.45%), indicates the precipitation of sulfates, such as gypsum, which is consistent with the structural observations in XRD. The correlation of these results with dissolution kinetics and post-leaching mineralogy confirms that the 20% condition promotes greater chemical reactivity of the system, while the 30% treatment partially preserves the original composition of the ore. Figure (8a) shows the trace elements, revealing a slight decrease in the concentration of Fe and Al after solubilization treatments, suggesting that these elements remain mostly in stable mineral phases. In contrast, elements such as Cu and Mn show a more marked reduction, especially in the 20% treatment, which could be attributed to mobilization or redistribution processes during the reaction. The relative stability of K, Sr, and Ti indicates that their behavior was not significantly affected, positioning them as possible indicators of the residual mineral structure. These results suggest that solubilization mainly affected the most labile elements or those associated with secondary phases.

One of the most notable findings is the divergence in the behavior of fluoride (F) depending on pulp density. In the 20% treatment, the residue retains high levels of F (≈18% Fig. 10a), acting as a residual structure. In contrast, in the deep reaction zone at 30% (Figure 10b, spectrum 2), the fluoride disappears completely. This phenomenon suggests that the higher density of the pulp generates microenvironments with extreme proton activity at the solid-liquid interface. Under these conditions, the chemical equilibrium shifts toward the formation of aqueous hydrofluoric acid (HF) or soluble fluorine complexes with traces of Al or Fe. This

suggests that biogenic acid not only contributes protons [49], but that secondary metabolites may facilitate the mobilization of halogens, which in conventional chemical acidulation systems tend to remain trapped in the solid phase.

The detection of 10.45% S by XRF, together with 22.16% Ca and only 0.23% P in the EDS at 30%, confirms the transformation of fluorapatite into biogenic gypsum $CaSO_4.2H_2O$. This process of pseudomorphism, in which the product replaces the reactant while maintaining the external shape of the grain, is fundamental to understanding the kinetics of the system [50].

The ability to achieve deep solubilization (reduction of P to 0.23% in internal cores) in less than 60 minutes suggests that acidulation mediated by *A. thiooxidans* metabolites is not limited by the kinetics of biological growth, but rather by mass transfer at the solid-liquid interface.

5. Conclusions

Biogenic leaching was validated as a highly effective method for recovering phosphorus from low-grade rock (5.5% P), achieving solubilization of over 98.7% in a single step. The use of *A. thiooxidans* allows resources of little commercial value to be transformed into strategic sources of nutrients under operating conditions with high pulp density (30%).

The data obtained show that there is an inverse correlation between pH and soluble phosphorus concentration, as well as a faster kinetic response in the system with a higher pulp concentration (30%). Therefore, it is concluded that the condition with 30% pulp allowed for more efficient solubilization in less time, reaching the maximum phosphorus concentration in a shorter time interval compared to the pulp density of 20%. This behavior suggests that, under certain conditions, an increase in the concentration of solids favors the immediate availability of phosphates in solution, possibly due to more intense surface dissolution mechanisms.

The dense morphological transition from the initial mineral to a structure with vacuolar porosity developed by leaching and a residual skeletal network represents physical evidence of a diffusion-controlled dissolution process, in which the phosphate matrix is removed for subsequent sulfate nucleation.

The specialized literature consistently shows that, in acidic or sulfate-enriched environments, the precipitation of $CaSO_4.2H_2O$ can form a crystalline film on carbonate minerals such as calcite or dolomite. This layer acts as a physical and chemical barrier, decreasing the transfer of H^+ ions and slowing down the dissolution of the substrate.

The results for a pulp density of 30% correspond to high substitution in the internal domains of the grain, as evidenced by the low residual phosphorus content (0.23%) detected by EDS. In line with this value, the high calcium content and absence of fluorine confirm the in-situ substitution of fluorapatite by calcium sulfate. Although FRX suggests apparent preservation of the composition, EDS reveals the formation of a reactive outer layer rich in phosphorus that encapsulates already leached cores. This behavior indicates the evolution of the system toward a core-shell structure, in which solubilization efficiency is partially masked by reaction byproducts.
Unlike conventional chemical methods, the biogenic route minimizes foaming and avoids classic passivation by acicular gypsum. The formation of a thin, permeable film allows the

reaction kinetics to be maintained at room temperature, eliminating the need for energy-intensive thermal processes.

This study lays a solid foundation for technological sovereignty in the use of complex phosphates. The process is in line with the circular economy by reducing the carbon footprint and water consumption and proposes a mineral biorefinery model applicable to deposits with energy or water constraints.

6. References

[1] H. A. Colorado, Z. Wang, and J.-M. Yang, “Inorganic phosphate cement fabricated with wollastonite, barium titanate, and phosphoric acid,” *Cem. Concr. Compos.*, vol. 62, pp. 13–21, Sep. 2015, doi: 10.1016/j.cemconcomp.2015.04.014.

[2] R. Florez, C. H. Castano Giraldo, S. M. Restrepo-Arcila, and H. A. Colorado, “Valorization of spent Zn-C battery and construction and demolition waste (CDW): Fabrication and characterization of geopolymer composites for radiation shielding applications,” *Open Ceramics*, vol. 18, p. 100588, Jun. 2024, doi: 10.1016/j.oceram.2024.100588.

[3] X. Liu *et al.*, “Application prospect of advanced oxidation technology in wet process phosphoric acid production,” *J. Environ. Chem. Eng.*, vol. 10, no. 6, Dec. 2022, doi: 10.1016/j.jece.2022.108868.

[4] Q. Liu *et al.*, “Study on reactions of gaseous P2O5 with Ca3(PO4)2 and SiO2 during a rotary kiln process for phosphoric acid production,” *Chin. J. Chem. Eng.*, vol. 26, no. 4, pp. 795–805, Apr. 2018, doi: 10.1016/j.cjche.2017.11.016.

[5] S. Abilkasova, S. Akhmetova, L. Kalimoldina, M. Suleimenova, A. Berkinbayeva, and G. Kabulova, “Study of the Process of Concentration of Wet-Process Phosphoric Acid on the Basis of Karatau Phosphorites,” Jul. 08, 2024. doi: 10.20944/preprints202407.0583.v1.

[6] H. Li *et al.*, “Control foaming performance of phosphate rocks used for wet-process of phosphoric acid production by phosphoric acid,” *Hydrometallurgy*, vol. 195, Aug. 2020, doi: 10.1016/j.hydromet.2020.105364.

[7] K. Lamghari, Y. Taha, Y. Ait-Khouia, A. Elghali, R. Hakkou, and M. Benzaazoua, “Sustainable phosphate mining: Enhancing efficiency in mining and pre-beneficiation processes,” *J. Environ. Manage.*, vol. 358, p. 120833, May 2024, doi: 10.1016/j.jenvman.2024.120833.

[8] A. Z. M. Abouzeid, “Physical and thermal treatment of phosphate ores - An overview,” Jan. 31, 2008. doi: 10.1016/j.minpro.2007.09.001.

[9] R. Yaoyang and H. Dongsheng, “Review on beneficiation and reagents used for Phosphate ores ,” *Minerals*, Apr. 2019.

[10] M. Jaganmohan, “Phosphate rock production worldwide in 2024, by country.”

[11] J. ’Moore, P. ’Nriagu, *Photosphate Minerals*. Berlin, Heidelberg: Springer Berlin Heidelberg, 1984. doi: 10.1007/978-3-642-61736-2.

[12] F. Hernáinz, M. Calero, and G. Blázquez, “Flotation of low-grade phosphate ore,” *Advanced Powder Technology*, vol. 15, no. 4, pp. 421–433, 2004, doi: 10.1163/1568552041270491.

[13] H. Amar, M. Benzaazoua, A. Elghali, R. Hakkou, and Y. Taha, “Waste rock reprocessing to enhance the sustainability of phosphate reserves: A critical review,” Dec. 25, 2022, *Elsevier Ltd*. doi: 10.1016/j.jclepro.2022.135151.

[14] H. Amar, M. Benzaazoua, A. Elghali, R. Hakkou, and Y. Taha, “Waste rock reprocessing to enhance the sustainability of phosphate reserves: A critical review,” Dec. 25, 2022, *Elsevier Ltd*. doi: 10.1016/j.jclepro.2022.135151.

[15] A. Z. M. Abouzeid, “Physical and thermal treatment of phosphate ores — An overview,” *Int. J. Miner. Process.*, vol. 85, no. 4, pp. 59–84, Jan. 2008, doi: 10.1016/J.MINPRO.2007.09.001.

[16] Y. Ruan, D. He, and R. Chi, “Review on beneficiation techniques and reagents used for phosphate ores,” Apr. 01, 2019, *MDPI AG*. doi: 10.3390/MIN9040253.

[17] A. Kumari, R. Panda, M. K. Jha, J. Y. Lee, J. R. Kumar, and V. Kumar, “Thermal treatment for the separation of phosphate and recovery of rare earth metals (REMs) from Korean monazite,” *Journal of Industrial and Engineering Chemistry*, vol. 21, pp. 696–703, Jan. 2015, doi: 10.1016/J.JIEC.2014.03.039.

[18] K. Schrödter, G. Bettermann, T. Staffel, F. Wahl, T. Klein, and T. Hofmann, “Phosphoric Acid and Phosphates,” in *Ullmann’s Encyclopedia of Industrial Chemistry*, Wiley, 2008. doi: 10.1002/14356007.a19_465.pub3.

[19] , Sandra Milena Restrepo Arcila, H. A. C. Lopera, and M. A. M. Godoy, “Orthophosphates Synthetized from Calcium and Calcium Magnesium Phosphates, Types of Resources and Applications: A Review,” *ES Materials and Manufacturing*, 2025, doi: 10.30919/mm1997.

[20] H. Li *et al.*, “Control foaming performance of phosphate rocks used for wet-process of phosphoric acid production by phosphoric acid,” *Hydrometallurgy*, vol. 195, Aug. 2020, doi: 10.1016/j.hydromet.2020.105364.

[21] T. S. do Carmo *et al.*, “Phosphorus Recovery from Phosphate Rocks Using Phosphate-Solubilizing Bacteria,” *Geomicrobiol. J.*, vol. 36, no. 3, pp. 195–203, Mar. 2019, doi: 10.1080/01490451.2018.1534901.

[22] A. Nobahar, E. T. Fitas, M. C. Costa, and J. D. Carlier, “Acid mine drainage bioremediation using bacteria enriched from the confluence zone between its flow and treated sewage,” *International Journal of Environmental Science and Technology*, vol. 22, no. 9, pp. 7487–7506, May 2025, doi: 10.1007/s13762-024-06160-z.

[23] R. Wang *et al.*, “Sulfur oxidation in the acidophilic autotrophic Acidithiobacillus spp.,” 2019, *Frontiers Media S.A.* doi: 10.3389/fmicb.2018.03290.

[24] G. R. Marlenne, M. V. Fernanda, and G. Rojas-Avelizapa Norma, “Acidithiobacillus thiooxidans DSM 26636: An alternative for the bioleaching of metallic burrs,” *Catalysts*, vol. 10, no. 11, pp. 1–11, Nov. 2020, doi: 10.3390/catal10111230.

[25] H. Hamidian, “Microbial Leaching of Uranium Ore,” 2011. [Online]. Available: www.intechopen.com

[26] O. I. Rzhepishevska, *Physiology and Genetics of Acidithiobacillus species: Applications for Biomining*. 2008.

[27] M. Gan, S. Zhou, M. Li, J. Zhu, X. Liu, and L. Chai, “Bioleaching of multiple heavy metals from contaminated sediment by mesophile consortium,” *Environmental Science and Pollution Research*, vol. 22, no. 8, pp. 5807–5816, Apr. 2015, doi: 10.1007/s11356-014-3759-x.

[28] B. Bayat and B. Sari, “Comparative evaluation of microbial and chemical leaching processes for heavy metal removal from dewatered metal plating sludge,” *J. Hazard. Mater.*, vol. 174, no. 1–3, pp. 763–769, Feb. 2010, doi: 10.1016/j.jhazmat.2009.09.117.

[29] S. Chen, J. Wu, and S. Sung, “Effects of sulfur dosage on continuous bioleaching of heavy metals from contaminated sediment.,” *J Hazard Mater.*, 2022, doi: 10.1016/j.jhazmat.2021.127257.

[30] M. Gan, S. Zhou, M. Li, J. Zhu, X. Liu, and L. Chai, “Bioleaching of multiple heavy metals from contaminated sediment by mesophile consortium,” *Environmental Science and Pollution Research*, vol. 22, no. 8, pp. 5807–5816, Apr. 2015, doi: 10.1007/s11356-014-3759-x.

[31] S. M. Calle-Castañeda, M. A. Márquez-Godoy, and J. P. Hernández-Ortiz, “Solubilization of phosphorus from phosphate rocks with Acidithiobacillus thiooxidans following a growing-then-recovery process,” *World J. Microbiol. Biotechnol.*, 2018, doi: 10.1007/s11274-017-2390-7.

[32] S. M. Calle-Castañeda, M. A. Márquez-Godoy, and J. P. Hernández-Ortiz, “Phosphorus recovery from high concentrations of low-grade phosphate rocks using the biogenic acid produced by the acidophilic bacteria Acidithiobacillus thiooxidans,” *Miner. Eng.*, 2018, doi: 10.1016/j.mineng.2017.10.014.

[33] M. P. Silverman' and D. G. Lundgren, "STUDIES ON THE CHEMOAUTOTROPHIC IRON BACTERIUM FERROBACILLUS FERROOXIDANS I. AN IMPROVED MEDIUM AND A HARVESTING PROCEDURE FOR SECURING HIGH CELL YIELDS," 1958. [Online]. Available: https://journals.asm.org/journal/jb

[34] ASTM International, "Standard Test Method for Sulfate Ion in Water.," 2023.

[35] ASTM International, "Standard Test Method for Sieve Analysis of Raw Materials for Glass Manufacture," 2001.

[36] Katarzyna J. Stanienda-Pilecki, "The Importance of Fourier-Transform Infrared Spectroscopy in the Identification of Carbonate Phases Differentiated in Magnesium Content," *Spectroscopy*, vol. 34, no. 6, Jan. 2019.

[37] J. D. Rodriguez-Blanco, S. Shaw, and L. G. Benning, "The kinetics and mechanisms of amorphous calcium carbonate (ACC) crystallization to calcite, via vaterite.," *Nanoscale*, vol. 3, no. 1, pp. 265–271, Jan. 2011, doi: 10.1039/c0nr00589d.

[38] Zhongxian Guo, Jibing Xiong, Muhammad Irfan Sohail, and Dejun Yang, "Investigating phosphorus release from lignite-based activated rock phosphate through TG-FTIR analysis," *Environ. Technol. Innov.*, vol. 23, Jul. 2021.

[39] P. Ptáček, "Identification, Characterization and Properties of Apatites," in *Apatites and their Synthetic Analogues - Synthesis, Structure, Properties and Applications*, InTech, 2016. doi: 10.5772/62211.

[40] L. Castro, F. González, A. Ballester, and C. García-Balboa, "Biohydrometallurgical Processes: A Practical Approach," 2011. [Online]. Available: https://www.researchgate.net/publication/261258766

[41] M. Sahadat Hossain, M. A. A. Shaikh, and S. Ahmed, "Synthesis of gypsum fertilizer from waste eggshells for a sustainable environment," *Mater. Adv.*, 2022, doi: 10.1039/d2ma00810f.

[42] H. A. Colorado, E. I. G. Velásquez, and S. N. Monteiro, "Sustainability of additive manufacturing: the circular economy of materials and environmental perspectives," *Journal of Materials Research and Technology*, vol. 9, no. 4, pp. 8221–8234, Jul. 2020, doi: 10.1016/j.jmrt.2020.04.062.

[43] A. Schippers, S. Hedrich, J. Vasters, M. Drobe, W. Sand, and S. Willscher, "Biomining: Metal Recovery from Ores with Microorganisms," 2013, pp. 1–47. doi: 10.1007/10_2013_216.

[44] J. Booth, Q. Hong, R. G. Compton, K. Prout, and R. M. Payne, "Gypsum Overgrowths Passivate Calcite to Acid Attack," 1997.

[45] A. Hernandez, A. La Rocca, H. Power, U. Graupner, and G. Ziegenbalg, "Modelling the effect of precipitation inhibitors on the crystallization process from well mixed over-saturated solutions in gypsum based on Langmuir-Volmer flux correction," *J. Cryst. Growth*, vol. 295, no. 2, pp. 217–230, Oct. 2006, doi: 10.1016/j.jcrysgro.2006.08.002.

[46] G. Yue, X. Zhu, G. Wang, and F. Ma, "Mineral Reaction Kinetics during Aciding of the Gaoyuzhuang Carbonate Geothermal Reservoir in the Xiong'an New Area, Northern China," *Water (Switzerland)*, vol. 14, no. 19, Oct. 2022, doi: 10.3390/w14193160.

[47] R. Lund, H. S. Foglerf, and C. C. Mccune, "Acidization-I. The dissolution of dolomite in hydrochloric acid," 1973.

[48] R. Zhang, S. Hu, X. Zhang, and W. Yu, "Dissolution kinetics of dolomite in water at elevated temperatures," *Aquat. Geochem.*, vol. 13, no. 4, pp. 309–338, Dec. 2007, doi: 10.1007/s10498-007-9022-z.

[49] A. C. Kanagalabavi, S. GD, K. M. D, and D. Patil, "Optimizing the solubility of low-grade rock phosphate to enable its use as a fertilizer in agriculture," *International Journal of Agriculture and Food Science*, vol. 7, no. 1, pp. 26–34, Jan. 2025, doi: 10.33545/2664844X.2025.v7.i1a.234.

[50] M. López, M. A. Alsina, L. Valderrama, and I. Nancucheo, "Bioleaching Phosphorus from Apatite Recovered from Iron Mine Tailings using Acidithiobacillus thiooxidans," *Journal of*

Sustainable Metallurgy, vol. 11, no. 4, pp. 3675–3684, Dec. 2025, doi: 10.1007/s40831-025-01074-7.